International Journal of Solids and Structures 45 (2008) 4936–4951

Contents lists available at ScienceDirect

International Journal of Solids and Structures

journal homepage: www.elsevier.com/locate/ijsolstr

Determination of mixed-mode stress intensity factors, fracture toughness, and crack turning angle for anisotropic foam material

Nagaraj K. Arakere [a,*], Erik C. Knudsen [a], Doug Wells [b], Preston McGill [b], Gregory R. Swanson [b]

[a] Mechanical & Aerospace Engineering Department, University of Florida, 237 MAE-B, Gainesville, FL 32611-6300, United States
[b] NASA Marshall Space Flight Center, Huntsville, AL-35812, United States

ARTICLE INFO

Article history:
Received 6 July 2007
Received in revised form 19 March 2008
Available online 11 May 2008

Keywords:
Foam
Anisotropy
Stress intensity factor
Mixed-mode loading
Fracture toughness
Crack turning angle
Anisotropic toughness

ABSTRACT

A numerical and experimental investigation for determining mixed-mode stress intensity factors, fracture toughness, and crack turning angle for BX-265 foam insulation material, used by NASA to insulate the external tank (ET) for the space shuttle, is presented. BX-265 foam is a type of spray-on foam insulation (SOFI), similar to the material used to insulate attics in residential construction. This cellular material is a good insulator and is very lightweight. Breakup of segments of this foam insulation on the shuttle ET impacting the shuttle thermal protection tiles during liftoff is believed to have caused the space shuttle Columbia failure during re-entry. NASA engineers are interested in understanding the processes that govern the breakup/fracture of this material from the shuttle ET. The foam is anisotropic in nature and the required stress and fracture mechanics analysis must include the effects of the direction dependence on material properties. Material testing at NASA Marshall Space Flight Center (MSFC) has indicated that the foam can be modeled as a transversely isotropic material. As a first step toward understanding the fracture mechanics of this material, we present a general theoretical and numerical framework for computing stress intensity factors (SIFs), under mixed-mode loading conditions, taking into account the material anisotropy. We present SIFs for middle tension – M(T) – test specimens, using 3D finite element stress analysis (ANSYS) and FRANC3D fracture analysis software. SIF values are presented for a range of foam material orientations. Mode I fracture toughness of the material is determined based on the SIF value at failure load. We also present crack turning angles for anisotropic foam material under mixed-mode loading. The results represent a quantitative basis for evaluating the strength and fracture properties of anisotropic foam insulation material.

1. Introduction

On February 1, 2003 the Space Shuttle Columbia suffered a catastrophic failure during re-entry. NASA has conducted an exhaustive investigation of the failure and the consensus now is that the breakup was caused by a segment of foam insulation, roughly the size of a suitcase, striking the wing during liftoff. The foam impact, in prior shuttle launches, has been known to cause impact damage to the thermal protection tiles, but was not considered to be a serious problem until the Columbia disaster. The damage to the thermal protection tiles in the leading edge of the wing is thought to have initiated thermal damage during re-entry, triggering a cascading series of catastrophic events that led to the loss of the shuttle.

The foam insulation is sprayed in layers on the cylindrical ET surface in liquid form which then expands and rises in the normal direction and a rind or knit line forms when the foam has settled and stops expanding. Referring to Fig. 1, the rise

* Corresponding author. Tel.: +1 352 392 0856: fax: +1 352 392 1071.
E-mail address: nagaraj@ufl.edu (N.K. Arakere).

0020-7683/$ - see front matter © 2008 Elsevier Ltd. All rights reserved.
doi:10.1016/j.ijsolstr.2008.04.028

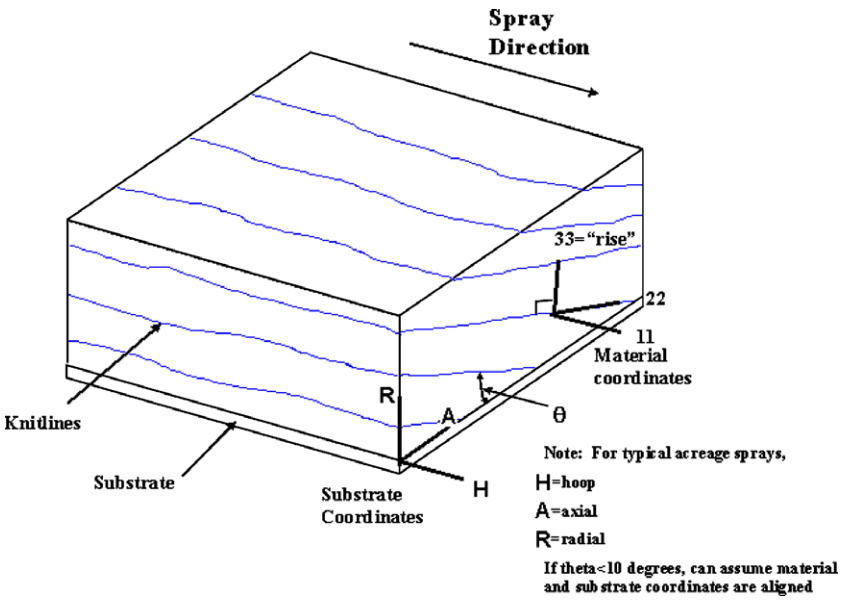

Fig. 1. Material coordinate system for spray-on foam insulation (SOFI).

direction is denoted by the 33 direction. The knit lines are also shown in Fig. 1. A second layer is then sprayed on and allowed to expand and the process continued until the insulation layer reaches the required thickness. Foam is a cellular material comprised of many individual cells at the microscopic level. During the spraying process, the sizes of the cells typically vary in the rise, axial and circumferential (hoop) directions, making the material properties direction dependent.

Certain areas of the ET have geometric discontinuities such as bolts, flanges, and fittings, as shown in Fig. 2. When the foam insulation is sprayed onto these areas voids can be created because of the geometric discontinuities. Furthermore, as the foam expands in these regions of, the rise directions normal to bolts and flanges will likely cause different material orientations and hence different anisotropic properties compared to areas that are relatively flat. The tank is filled with liquid oxygen and hydrogen and therefore the foam is exposed to cryogenic temperatures at the ET's surface. Liquid nitrogen and oxygen (air) can condense into any voids present. During liftoff the outer surface of the foam is exposed to aerodynamic heating. This heating is thought to raise the temperature of the liquid nitrogen, turning it into a gas. The pressure difference associated with the formation of the gas can cause pieces of foam to be blown out during liftoff.

NASA MSFC has undertaken extensive testing to measure the elastic and fracture properties of the BX-265 foam that insulates the ET. Fig. 3 shows the middle tension – M (T) – fracture specimen used for evaluating fracture toughness. Fig. 4 shows the tensile test specimens used for determining elastic constants. NASA is performing an investigation to study the effects of material orientation on strength and fracture properties of the foam material. Evaluating the variation of SIF, fracture toughness, and crack turning angle, as a function of material orientation is a first step towards a broader understanding of the failure processes of the foam material at certain critical areas of the shuttle ET containing bolts, flanges, and fittings.

A wide range of bending, shear, and tensile tests were performed at NASA MSFC, to obtain the elastic properties of foam, shown in Table 1. The tensile load–deflection behavior showed that the foam behaves as a brittle material and fractures with small deformation. Although foam is a cellular material comprised of many individual cells at the microscopic level, for the purposes of this initial investigation, we will assume that the material behaves as a homogeneous anisotropic elastic solid and follows laws of linear elastic fracture mechanics. Based on elastic properties shown in Table 1 this material can be approximated as a transversely isotropic material, with the plane of isotropy being 11–22. The material coordinate system used to define the transverse isotropy is shown in Fig. 5. The foam material is stiffer in the rise direction than the axial and hoop directions.

The objectives for this paper are to present a general numerical and experimental procedure for evaluating mixed-mode SIF (K_I, K_{II}, K_{III}), fracture toughness for a M(T) foam specimen shown in Fig. 3, and crack turning angle, as a function of material orientation, considering the foam as a transversely isotropic material.

2. Computation of stress intensity factors for cracks in anisotropic materials

The computation of SIFs for cracks subjected to mixed-mode loading in isotropic elastic solids can be accomplished in a straightforward manner using a number of analytical and numerical methods. Aliabadi and Rooke (1991) present a detailed summary of available methods for analytical and numerical evaluation of SIFs in isotropic materials. Some commonly used

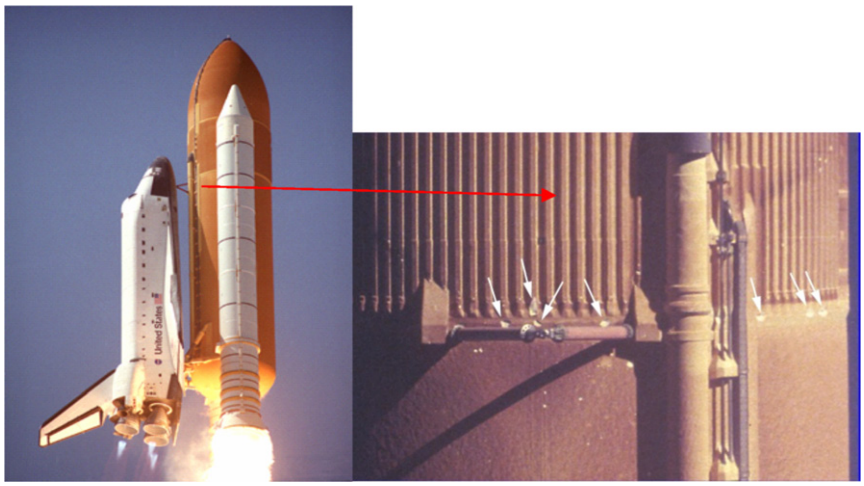

Fig. 2. Areas on the shuttle ET, with geometric discontinuities, that are prone for loss of foam insulation material during liftoff.

Fig. 3. Middle tension, M(T), fracture test specimen used at NASA MSFC.

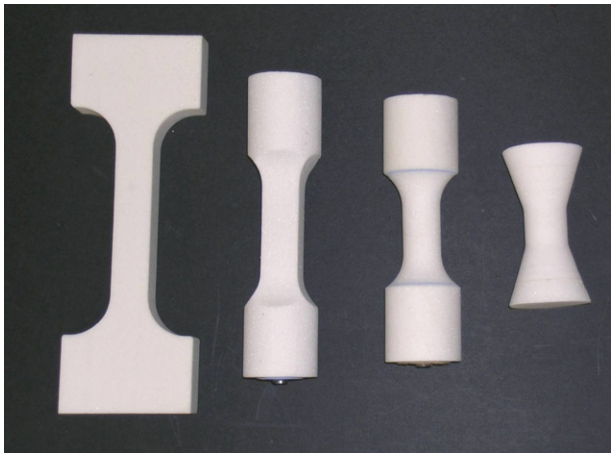

Fig. 4. Foam tensile test specimens used for determining elastic constants.

Table 1
Experimentally measured material elastic constants

E_{11} = 950 psi (6.55 MPa)	ν_{12} = 0.45	G_{12} = 328 psi (2.26 MPa)
E_{22} = 950 psi (6.55 MPa)	ν_{23} = 0.3	G_{23} = 231 psi (1.59 MPa)
E_{33} = 2400 psi (16.54 MPa)	ν_{13} = 0.3	G_{31} = 231 psi (1.59 MPa)

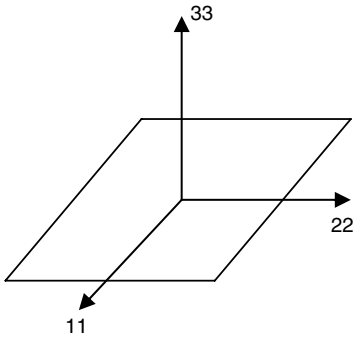

Fig. 5. Coordinate system used for the transversely isotropic foam material, with 33 as the foam rise direction.

methods are the *J*-integral approach (Rice, 1968), virtual crack extension (Parks, 1974; Ishikawa, 1980), modified crack closure integral and displacement extrapolation methods (Raju, 1987). However, none of these methods can be used for obtaining *K*-solutions for a crack in a general anisotropic solid subject to mixed-mode loading (see Fig. 6).

For a crack front subjected to mixed-mode loading, near-tip displacement fields are a linear combination of the three deformation modes. For general anisotropy there is full coupling between K_I, K_{II}, K_{III} and the three modes of deformation. For *z*-symmetry (plane of material symmetry is perpendicular to the crack front), there is decoupling between the in plane (*x*–*y* plane (K_I, K_{II})) and out of plane deformations (K_{III}). For isotropy there is complete decoupling between the three deformation modes with respect to the *K*-solutions. Ranjan and Arakere (2008) have presented mixed-mode SIFs for a *z*-symmetry crack in a FCC single crystal material. FCC single crystals have cubic symmetry requiring three independent elastic constants to relate stress and strain.

Sih et al. (1965) presented the stress and displacement fields near a crack tip for the case of *z*-symmetry. Hoenig (1982) presented the stress and displacement fields near a crack tip for general anisotropy. The concept of a *M*-integral, $M^{(1,2)}$ (Yau et al., 1980) is based on the linear superposition of two separate and independent equilibrium states. Banks-Sills et al. (2007) draw upon the work of Sih et al. (1965), Hoenig (1982), Yau et al. (1980), Li et al. (1985) and Banks-Sills et al. (2005) and present a comprehensive numerical framework for computing SIFs for cracks in anisotropic materials, which form the basis for the current FRANC3D FEA based fracture analysis code developed by the Cornell University fracture group (FRANC3D Concepts and Users Guide, 2003). Earlier versions of FRANC2D and FRANC3D, based on work by Swenson and Ingraffea (1987, 1988a,b), were primarily used for isotropic materials. With an adaptive mesh technique, this fracture software can simulate crack growth without prescribing the crack path. Their work has provided fundamental understandings for the simulation of dynamic crack propagation based on FEA. We present a brief synopsis of the pertinent equations necessary for evaluating SIF's under mixed-mode loading for anisotropic materials, based on Banks-Sills et al. (2007). Rice's *J*-integral (Rice, 1968) represents the energy flux into the crack tip region, and is equal to the energy release rate under conditions of small-scale yielding. The three-dimensional form of the *J*-integral was first presented by Shih et al. (1986) and later re-derived by

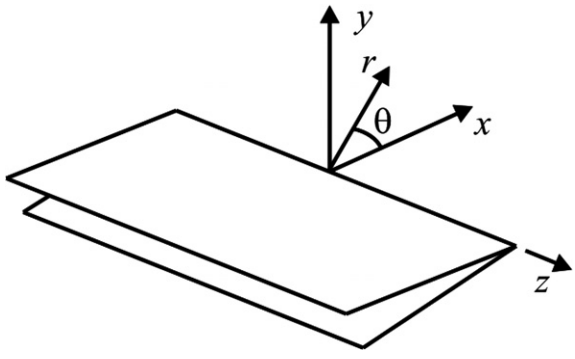

Fig. 6. Coordinate system used for the local crack front.

Freed and Banks-Sills (2005), and is reproduced here as

$$\int_0^{L_N} G(z) l_x^{(N)}(z) n_x \mathrm{d}z = \int_V \left[\sigma_{ij}\frac{\partial u_i}{\partial x_1} - W\delta_{1j}\right]\frac{\partial q_1}{\partial x_j}\mathrm{d}V \tag{1}$$

where G is the energy release rate along the crack front, $\delta l = l_x^{(N)} n_x$ is the normalized virtual crack extension orthogonal to the crack front, n_x is the unit normal to the crack front in the x-direction, N represents the element number N along the crack front, and L_N is its length, $W = \sigma_{ij}\varepsilon_{ij}/2$ is the strain energy density, and δ_{ij} is the Kronecker delta. The subscripts i and j are used to represent crack tip coordinates x, y and z, andσ_{ij}, ε_{ij} and u_i represent the stress, strain and displacement components in the crack tip coordinate system. This form of the J-integral was utilized to derive a three-dimensional form of the M-integral (Banks-Sills et al. (2007)) for the general anisotropic case, as

$$M^{(1,2\alpha)} = \frac{1}{A_\mathrm{q}}\int_V \left[\sigma_{ij}^{(1)}\frac{\partial u_i^{(2\alpha)}}{\partial x_1} + \sigma_{ij}^{(2\alpha)}\frac{\partial u_i^{(1)}}{\partial x_1} - W^{(1,2\alpha)}\delta_{1j}\right]\frac{\partial q_1}{\partial x_j}\mathrm{d}V \tag{2}$$

where $\alpha = a$, b and c in succession, the area of virtual crack extension is given by

$$A_\mathrm{q} = \int_0^{L_N} l_x^{(N)}(z)\mathrm{d}z \tag{3}$$

and the interaction energy density

$$W^{(1,2\alpha)} = \sigma_{ij}^{(1)}\varepsilon_{ij}^{(2\alpha)} = \sigma_{ij}^{(2\alpha)}\varepsilon_{ij}^{(1)} \tag{4}$$

The M-integral describes the interaction between the two equilibrium states, denoted by the superscripts 1 and 2, which can be superposed since the material is linearly elastic. The function q is one at the crack tip and zero on the arbitrary boundary surface S that defines the volume V of the integration domain, and can be interpreted as a virtual crack extension (Freed and Banks-Sills (2005)). The relationship between the average value of M through the element thickness, denoted by $\overline{M}$, and the stress intensity factors for a straight crack in a general anisotropic solid for which the material and crack coordinates may be at arbitrary angles, is given below (Banks-Sills et al., 2007)

$$\overline{M}^{(1,2a)} = -\frac{1}{2A_\mathrm{q}}\left\{2K_\mathrm{I}^{(1)}\mathrm{Im}\left(m_{2i}N_{i1}^{-1}\right) + K_\mathrm{II}^{(1)}\mathrm{Im}\left(m_{1i}N_{i1}^{-1} + m_{2i}N_{i2}^{-1}\right) + K_\mathrm{III}^{(1)}\mathrm{Im}\left(m_{3i}N_{i1}^{-1} + m_{2i}N_{i3}^{-1}\right)\right\} \tag{5}$$

$$\overline{M}^{(1,2b)} = -\frac{1}{2A_\mathrm{q}}\left\{K_\mathrm{I}^{(1)}\mathrm{Im}\left(m_{2i}N_{i2}^{-1} + m_{1i}N_{i1}^{-1}\right) + 2K_\mathrm{II}^{(1)}\mathrm{Im}\left(m_{1i}N_{i2}^{-1}\right) + K_\mathrm{III}^{(1)}\mathrm{Im}\left(m_{3i}N_{i2}^{-1} + m_{1i}N_{i3}^{-1}\right)\right\} \tag{6}$$

$$\overline{M}^{(1,2c)} = -\frac{1}{2A_\mathrm{q}}\left\{K_\mathrm{I}^{(1)}\mathrm{Im}\left(m_{2i}N_{i3}^{-1} + m_{3i}N_{i1}^{-1}\right) + K_\mathrm{II}^{(1)}\mathrm{Im}\left(m_{1i}N_{i3}^{-1} + m_{3i}N_{i2}^{-1}\right) + 2K_\mathrm{III}^{(1)}\mathrm{Im}\left(m_{3i}N_{i3}^{-1}\right)\right\} \tag{7}$$

Eqs. (5)–(7), expressed in matrix form, lead to the relationship between stress intensity factors and $\overline{M}$, shown below:

$$\begin{bmatrix} 2\mathrm{Im}\left(m_{2i}N_{i1}^{-1}\right) & \mathrm{Im}\left(m_{1i}N_{i1}^{-1} + m_{2i}N_{i2}^{-1}\right) & \mathrm{Im}\left(m_{3i}N_{i1}^{-1} + m_{2i}N_{i3}^{-1}\right) \\ \mathrm{Im}\left(m_{2i}N_{i2}^{-1} + m_{1i}N_{i1}^{-1}\right) & 2\mathrm{Im}\left(m_{1i}N_{i2}^{-1}\right) & \mathrm{Im}\left(m_{3i}N_{i2}^{-1} + m_{1i}N_{i3}^{-1}\right) \\ \mathrm{Im}\left(m_{2i}N_{i3}^{-1} + m_{3i}N_{i1}^{-1}\right) & \mathrm{Im}\left(m_{1i}N_{i3}^{-1} + m_{3i}N_{i2}^{-1}\right) & 2\mathrm{Im}\left(m_{3i}N_{i3}^{-1}\right) \end{bmatrix}\begin{Bmatrix} K_\mathrm{I}^{(1)} \\ K_\mathrm{II}^{(1)} \\ K_\mathrm{III}^{(1)} \end{Bmatrix} = -2A_\mathrm{q}\begin{Bmatrix} \overline{M}^{(1,2a)} \\ \overline{M}^{(1,2b)} \\ \overline{M}^{(1,2c)} \end{Bmatrix} \tag{8}$$

The parameters m_{ij} are given by

$$\begin{aligned} m_{1i} &= S'_{11}\mu_i^2 - S'_{16}\mu_i + S'_{12} + \lambda_i\left(S'_{15}\mu_i - S'_{14}\right) \\ m_{2i} &= S'_{21}\mu_i - S'_{26} + S'_{22}/\mu_i + \lambda_i\left(S'_{25} - S'_{24}/\mu_i\right) \\ m_{3i} &= S'_{41}\mu_i - S'_{46} + S'_{42}/\mu_i + \lambda_i\left(S'_{45} - S'_{44}/\mu_i\right) \end{aligned} \tag{9}$$

where, under plane strain condition $S'_{ij} = S_{ij} - (S_{i3}S_{3j}/S_{33})$, and S_{ij} ($i,j = 1, \ldots, 6$) is the contracted material compliance matrix obtained from the fourth order tensor S_{ijkl} ($i, j, k, l = 1, 2, 3$) and $\varepsilon_{ij} = S_{ijkl}\sigma_{kl}$ (Ting, 1996).

The parameters μ_i ($i = 1, 2, 3$) are the roots of the sixth order characteristic equation of the plane strain compliance matrix given as

$$l_4(\mu)l_2(\mu) - l_3^2(\mu) = 0 \tag{10}$$

where

$$\begin{aligned} l_2(\mu) &= S'_{55}\mu^2 - 2S'_{45}\mu + S'_{44} \\ l_3(\mu) &= S'_{15}\mu^3 - \left(S'_{14} + S'_{56}\right)\mu^2 + \left(S'_{25} + S'_{46}\right)\mu - S'_{24} \\ l_4(\mu) &= S'_{11}\mu^4 - 2S'_{16}\mu^3 + \left(2S'_{12} + S'_{66}\right)\mu^2 - 2S'_{26}\mu + S'_{22} \end{aligned}$$

The roots μ_i ($i = 1, 2, 3$) occur in complex conjugate pairs and the three roots with positive imaginary parts are selected. The matrix N_{ij} (singular for isotropy and z-symmetry) is given by

$$N_{ij} = \begin{bmatrix} 1 & 1 & 1 \\ -\mu_1 & -\mu_2 & -\mu_3 \\ -\lambda_1 & -\lambda_2 & -\lambda_3 \end{bmatrix} \tag{11}$$

The parameters λ_i are given by

$$\lambda_i = -\frac{l_3(\mu_i)}{l_2(\mu_i)}, \quad i = 1, 2, 3 \tag{12}$$

A transversely isotropic linear elastic solid has 5 independent elastic constants given in Table 1. The relationship between the constants, with the plane of isotropy being 11–22 (Fig. 5), are $E_{11} = E_{22}$, $G_{23} = G_{13}$, $v_{12} = v_{21}$, $G_{12} = E_{11}/\{2(1 + v_{12})\}$ and $\frac{v_{ij}}{E_j} = \frac{v_{ji}}{E_i}$ (summation not implied). The strain–stress relations are given as

$$\begin{Bmatrix} \varepsilon_{11} \\ \varepsilon_{22} \\ \varepsilon_{33} \\ \gamma_{23} \\ \gamma_{13} \\ \gamma_{12} \end{Bmatrix} = \begin{bmatrix} \frac{1}{E_1} & \frac{-v_{12}}{E_2} & \frac{-v_{13}}{E_3} & 0 & 0 & 0 \\ \frac{-v_{21}}{E_1} & \frac{1}{E_2} & \frac{-v_{23}}{E_3} & 0 & 0 & 0 \\ \frac{-v_{31}}{E_1} & \frac{-v_{32}}{E_2} & \frac{1}{E_3} & 0 & 0 & 0 \\ 0 & 0 & 0 & \frac{1}{G_{23}} & 0 & 0 \\ 0 & 0 & 0 & 0 & \frac{1}{G13} & 0 \\ 0 & 0 & 0 & 0 & 0 & \frac{1}{G_{12}} \end{bmatrix} \begin{Bmatrix} \sigma_{11} \\ \sigma_{22} \\ \sigma_{33} \\ \sigma_{23} \\ \sigma_{13} \\ \sigma_{12} \end{Bmatrix} \tag{13}$$

Eq. (8) provides the basis for computing SIFs, provided that a numerical procedure is implemented for computing the M-integrals in the RHS vector. The fracture code FRANC3D has been set up to take the displacement and stress field input from a anisotropic FEA crack mesh model using commercial software such as ANSYS or ABAQUS, compute the elements of the matrix and M-integral RHS vector in Eq. (8), and solve for the K values along the crack front. This entails the following steps (Knudsen, 2006; Knudsen and Arakere, 2006): (a) computation of material compliance and stiffness matrices and rotating them into the global model coordinate system, (b) determination of a local crack front coordinate system and translation and rotation of all crack front coordinates into the local system, (c) determination of the material class in the rotated configuration, i.e. isotropy, z-symmetry or general anisotropy, (d) computation of μ_i for z-symmetry or μ_i, λ_i, m_{ij}, and N^{-1} for general anisotropy, (e) computation of auxiliary displacements at the crack front using analytical expressions, (f) computation of displacement derivatives at the integration points, (g) computation of stresses at the integration points from the analytical expressions, (i) integrate numerically to determine the M-integrals, (j) compute the area of the virtual crack extension, (k) solve Eq. (8) for the unknown stress intensity factors.

3. Finite element analysis

A middle tension M(T) specimen loaded in tension was modeled using ANSYS commercial finite element software (ANSYS Elements Reference, 1999), shown in Fig. 7. The specimen is 12 in. (305 mm) long, 5.5 in. (140 mm) wide and 1.5 in. (38 mm) thick. The center crack in the foam is cut with a razor blade. The 3D model is comprised entirely of SOLID92 and SOLID95 elements with the ability to account for material anisotropy. A 1-psi (6895 Pa) tensile normal stress was applied to the top face of the model. This results in an 8.25 lb (36.7 N) tensile load being applied to the specimen, since the area of cross section of the specimen is 8.25 in^2 (0.00532 m^2). We compute the SIFs for this load and since SIF scales linearly with load, we can readily estimate K values for other loads. Based on the fracture load for the test specimen, we can then estimate the fracture toughness for the material.

4. Material orientation

There is potential for variation of material orientation relative to the ET, in regions of geometric discontinuities such as bolts and flanges since the foam rise direction will not be normal to the ET surface, as shown in Fig. 8. To perform a systematic study of variation of material orientation we adopt a system illustrated in Fig. 9. The inner cone with the yellow dots has an included angle of 60° and the outer cone with the blue dots has an included angle of 90°. The numbered dots indicate case numbers, 0-8 and 9–16, and represent specific material orientations. Case 0 corresponds to the Z-axis with no tilt, i.e. there is no relative offset between the substrate and the material coordinate system. For each case the Z'-axis passes through that numbered dot and this can be achieved by appropriate rotations about the X and Y' axes. For example, case 1, shown by ($X'Y'Z'$) in Fig. 9, represents the material orientation with the Z' axis passing through the point 1 of the inner cone, obtained by a positive rotation about the X-axis by 30°. Similarly, material orientation for case 2 is obtained by a positive rotation about the X-axis by 22.2° and a (negative) rotation about the Y'-axis by −22.2°. The required rotations about the X and Y' axes for all 17 cases are listed in Table 2. The 17 material orientations analyzed are considered to encompass most variations encountered during the spraying of all parts of the ET.

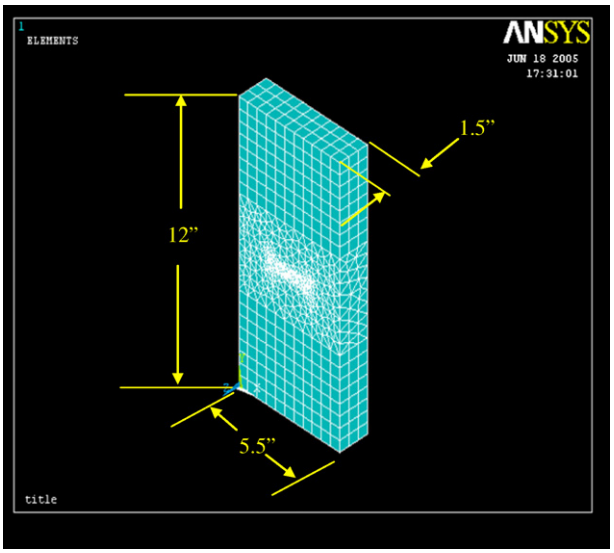

Fig. 7. Middle tension M(T) test specimen model built in ANSYS.

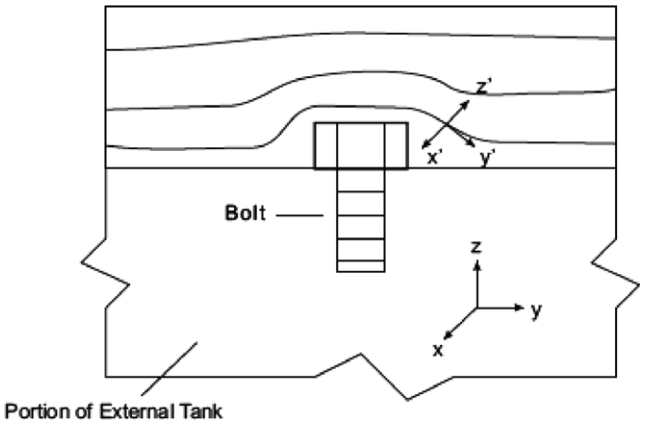

Fig. 8. Variation of material orientation relative to the ET.

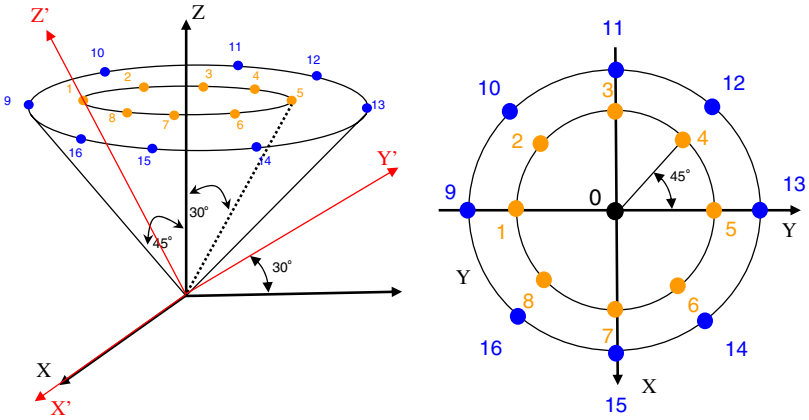

Fig. 9. Specific foam material orientations selected for analysis. The ($X'Y'Z'$) material orientation represents case 1, with the Z' axis tilting 30° to the Z-axis. (For interpretation of the references to color in this figure citation, the reader is referred to the web version of the article.)

Table 2
Specimen mid plane K_I values for crack inclination $\phi = 0°$

Case number	K_I(Pa$\sqrt{m}$)	K_I(psi$\sqrt{in.}$)	X-axis rotation (°)	Y'-axis rotation (°)
0	2187	1.99	0	0
1	2209	2.01	30	0
2	2352	2.14	22.2	−22.2
3	**2473**	**2.25**	0	−30
4	2352	2.14	−22.2	−22.2
5	2209	2.01	−30	0
6	2352	2.14	−22.2	22.2
7	**2473**	**2.25**	0	30
8	2352	2.14	22.2	22.2
9	2275	2.07	45	0
10	2407	2.19	35.3	−35.3
11	**2495**	**2.27**	0	−45
12	2407	2.19	−35.3	−35.3
13	2275	2.07	−45	0
14	2407	2.19	−35.3	35.3
15	**2495**	**2.27**	0	45
16	2407	2.19	35.3	35.3

Mean $K_I = 2360$ Pa$\sqrt{m}$ (2.148 psi$\sqrt{in.}$) [$a = 0.254$ m (1 in.), $\sigma = 6895$ Pa (1 psi), 1 psi$\sqrt{in.} = 1099$ Pa$\sqrt{m}$].

The material orientation for case 1 is further explained in Fig. 10. The local or primed coordinate system is obtained by a positive 30° rotation about the X-axis. This corresponds to the knit lines in the foam oriented at a 30° angle to the y-axis. The direction cosines to the primed system for cases 0–16, required for stress transformations between the primed and unprimed systems, can be readily obtained using the rotations listed in Table 2.

5. Stress intensity factor results

Finite element models were run in ANSYS for the 17 material orientations defined in Fig. 9, using the material properties defined in Table 1, and the displacement and stress field results input to FRANC3D for post-processing and computation of SIFs. Crack inclination angle to the horizontal, ϕ, of 0 and 30° were used. Stress intensity factors are presented as a function of normalized crack front distance or distance through the thickness, with 'zero' indicating the front face and 'one' indicating the specimen back face. Fig. 11 shows the mode I SIF for zero degree crack inclination, for cases 0 and 1–4, for a far-field loading $\sigma = 1$ psi (6895 Pa). Since the foam material is a lightweight and low strength material, a very low far field loading of $\sigma = 1$ psi (6895 Pa) is used. Again, this corresponds to an 8.25 lb (36.7 N) tensile load applied to the 12 in. (305 mm) long, 5.5 in. (140 mm) wide and 1.5 in. (38 mm) thick test specimen with crack length $a = 0.0254$ m (1 in.). Cases 0, 1 and 3 have symmetric K_I values as a function of thickness, while cases 2 and 4 are anti symmetric with respect to each other. The symmetric cases have a maximum K_I value at the specimen mid plane. K_I values at the specimen mid plane in Fig. 11 vary from 2 psi$\sqrt{in.}$(2198 Pa$\sqrt{m}$) to 2.25 psi$\sqrt{in.}$(2473 Pa$\sqrt{m}$). Fig. 12 shows K_I results for mode I SIF for a 30° crack inclination, for cases 0 and 1–4. Figs. 13 and 14 show K_{II} and K_{III} values for a 30° crack inclination, for cases 0 and 1–4.

The mid-plane K_I values for zero degree crack inclination, shown in Table 2, are examined in further detail, for all 17 cases analyzed. Case 0 has a minimum K_I value of 1.99 psi$\sqrt{in.}$(2187 Pa$\sqrt{m}$). Cases 3 and 7 (for the 30° cone) and corresponding cases 11 and 15 (for the 45° cone) exhibit the maximum K_I values of 2.25 psi$\sqrt{in.}$(2473 Pa$\sqrt{m}$) and 2.27 psi$\sqrt{in.}$(2495 Pa$\sqrt{m}$), respectively. This represents a 14% difference between the minimum (case 0) and maximum

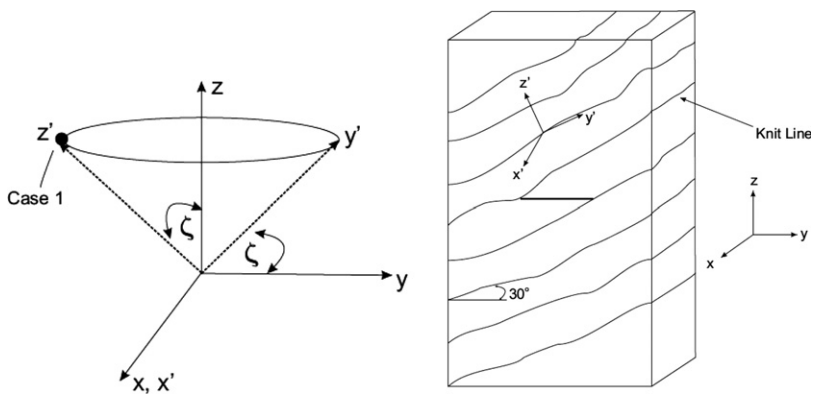

Fig. 10. Definition of case one material orientation for the M(T) FE model.

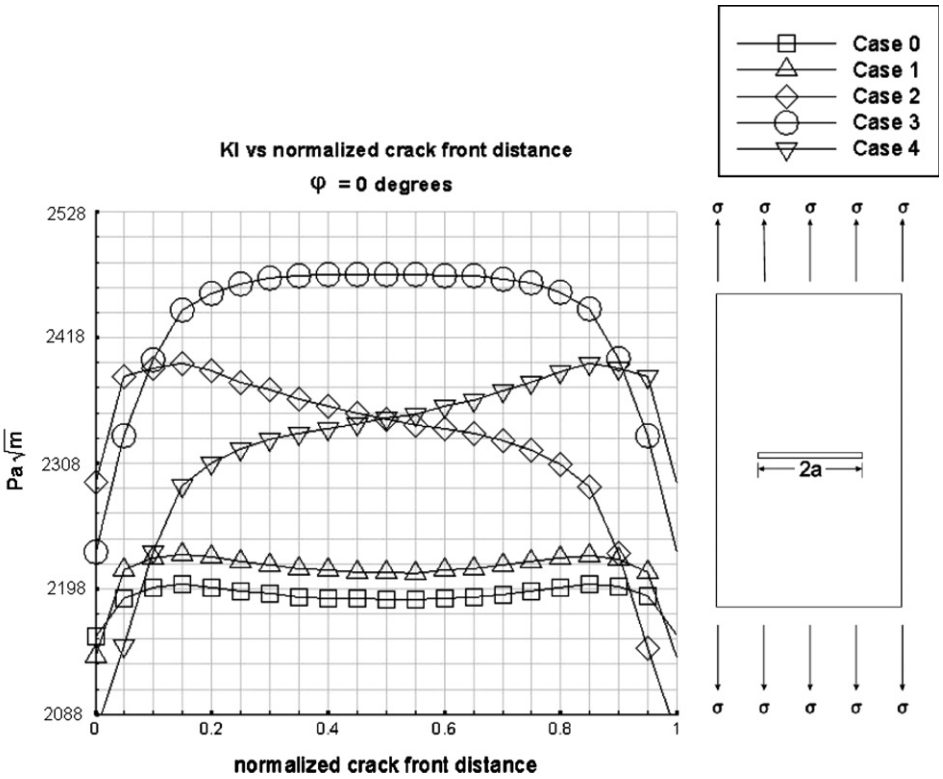

Fig. 11. Mode I SIF (K_I) for cases 0 and 1–4; crack inclination $\phi = 0°$. [$a = 0.254$ m (1 in.), $\sigma = 6895$ Pa (1 psi)].

(cases 11 and 15, 45° inclination in rise direction) K_I value, indicating that the K_I values are not very sensitive to change in material orientation.

6. Anisotropic fracture toughness

Fracture toughness can be estimated based on the failure load of M(T) specimen and scaling the K_I value linearly with applied load. The failure load for 3 M(T) test specimens with a zero degree crack inclination, and approximately case 0 orientation are 85 lb (378 N), 95 lb (422 N), and 106 lb (471 N). The K_I value for case 0 with an applied tensile load of 8.25 lb (36.7 N) is $1.99\ \text{psi}\sqrt{\text{in.}}(2187\ \text{Pa}\sqrt{\text{m}})$. Scaling linearly with load, this yields fracture toughness values of $\frac{85}{8.25} * 1.99 = 20.5\ \text{psi}\sqrt{\text{in.}}(22,530\ \text{Pa}\sqrt{\text{m}})$, $\frac{95}{8.25} * 1.99 = 22.9\ \text{psi}\sqrt{\text{in.}}(25,167\ \text{Pa}\sqrt{\text{m}})$, and $\frac{106}{8.25} * 1.99 = 25.5\ \text{psi}\sqrt{\text{in.}}(28,025\ \text{Pa}\sqrt{\text{m}})$, respectively. The mean fracture toughness value from the three data points is $23\ \text{psi}\sqrt{\text{in.}}(25,277\ \text{Pa}\sqrt{\text{m}})$. Using the mean K_I value from Table 2 [$2360\ \text{Pa}\sqrt{\text{m}}(2.148\ \text{psi}\sqrt{\text{in.}})$] as a scaling factor to account for variation in material orientation, instead of $1.99\ \text{psi}\sqrt{\text{in.}}(2187\ \text{Pa}\sqrt{\text{m}})$ for case 0 orientation alone yields a mean fracture toughness of $\frac{2.148}{1.99} * 23 = 24.8\ \text{psi}\sqrt{\text{in.}}(27,255\ \text{Pa}\sqrt{\text{m}})$. From these arguments, a mode I plane strain fracture toughness value in the rise (33) direction between 23 and $25\ \text{psi}\sqrt{\text{in.}}(25,277 - -27,475\ \text{Pa}\sqrt{\text{m}})$ is a reasonable figure for the BX-265 foam material. Based on additional testing, the fracture toughness in the 11 and 22 directions is estimated to be $17.4\ \text{psi}\sqrt{\text{in.}}(19,122\ \text{Pa}\sqrt{\text{m}})$ and $19.5\ \text{psi}\sqrt{\text{in.}}(21,430\ \text{Pa}\sqrt{\text{m}})$. It is worth noting that the units are in $psi\sqrt{\text{in.}}(\text{Pa}\sqrt{\text{m}})$ and *not* $\text{ksi}\sqrt{\text{in.}}(\text{MPa}\sqrt{\text{m}})$.

In general, materials may exhibit elastic anisotropy as well as anisotropy in fracture resistance. Many materials are virtually isotropic elastically, but have a preferred direction of (mode I) crack propagation resulting from the manner in which the material is processed. If the processing is of symmetric character, as for rolled sheet or plate, the two-dimensional relation describing the crack growth resistance as a function of orientation has two axes of symmetry. For convenience, the orientation describing the crack angle in material coordinates is measured from the longitudinal grain direction, which corresponds to the rolling direction for rolled products. The crack growth resistance is maximum for growth across the rolling direction ($\theta = 90°$, or L–T) and minimum for growth parallel to the rolling direction (0°, or T–L) (Lemant and Pineau, 1981). For this case of two-dimensional fracture orthotropy, in the context of a maximum stress theory, Buczek and Herakovich (1985) proposed a fracture orthotropy interpolation function by requiring that the toughness function be independent of θ for isotropic materials, and that it possess the desired orthogonal symmetry, collocating to K_p (0°) and K_p (90°) values, and is given by

$$K_p(\theta) = K_p(0°)\cos^2\theta + K_p(90°)\sin^2\theta \tag{14}$$

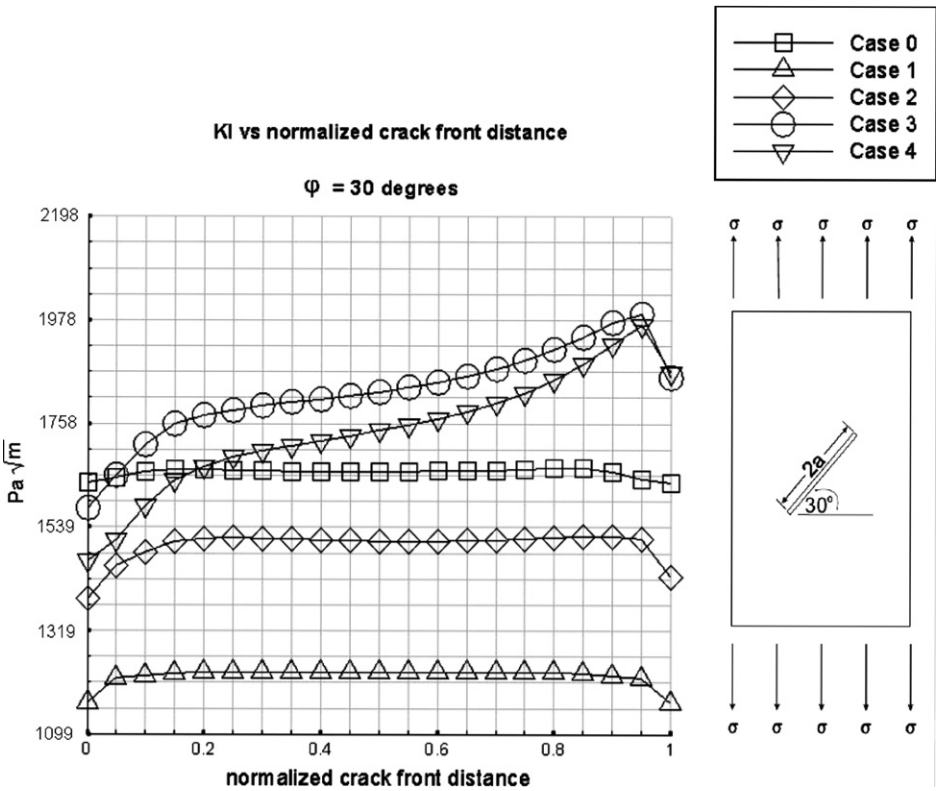

Fig. 12. Mode I SIF (K_I) for cases 0 and 1–4; crack inclination $\phi = 30°$. [$a = 0.254$ m (1 in.), $\sigma = 6895$ Pa (1 psi)].

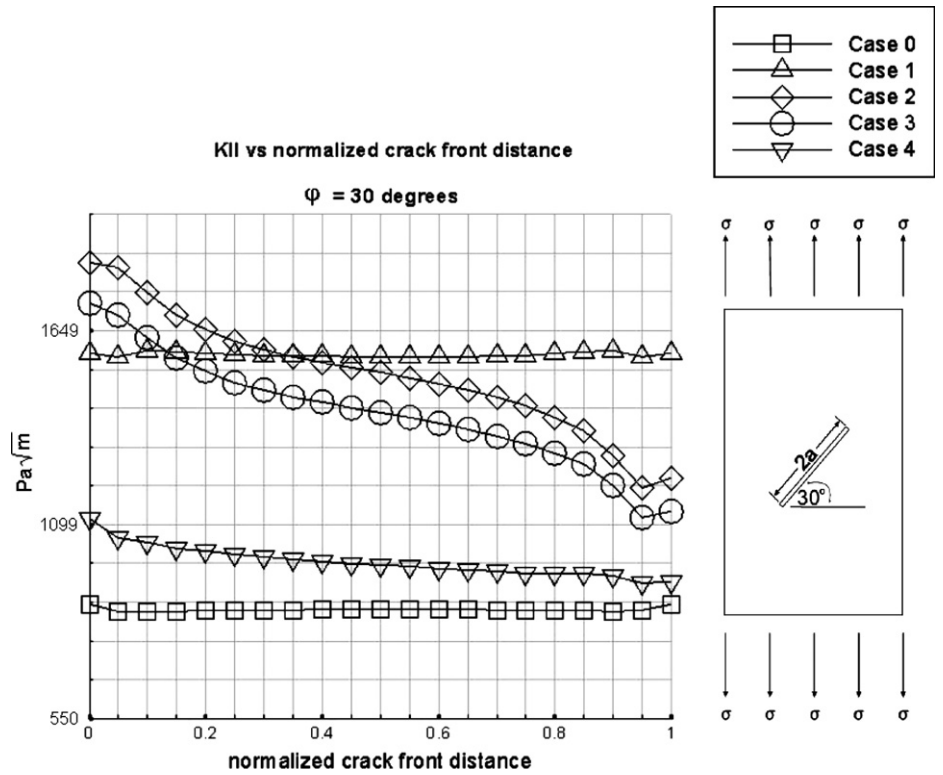

Fig. 13. Mode II SIF (K_{II}) for cases 0 and 1–4; crack inclination $\phi = 30°$. [$a = 0.254$ m (1 in), $\sigma = 6895$ Pa (1 psi)].

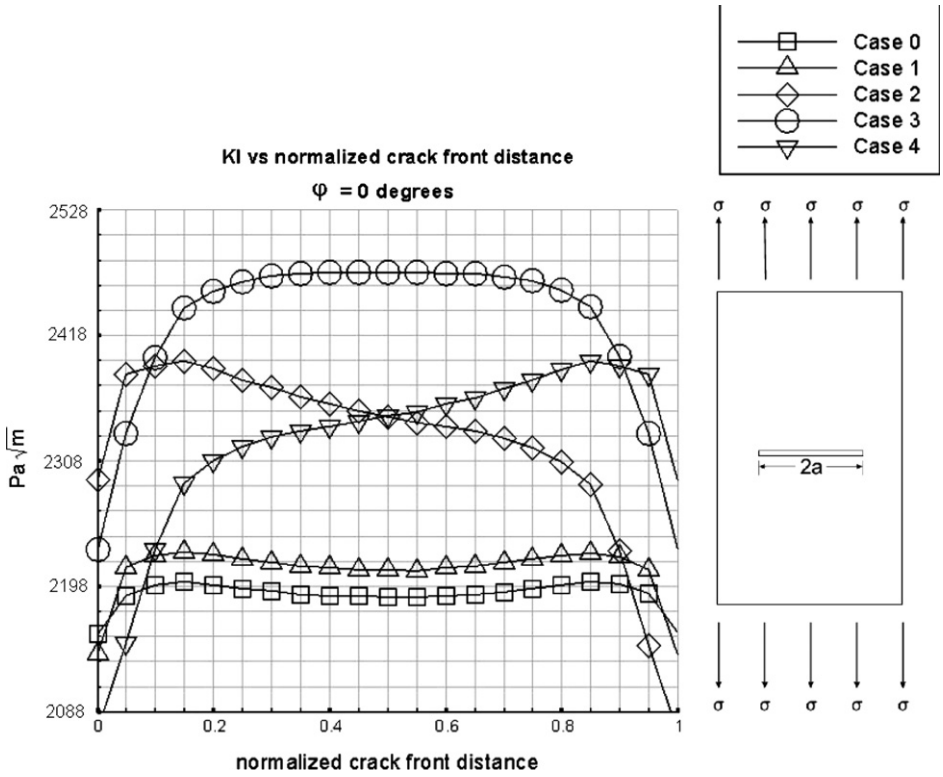

Fig. 14. Mode III SIF (K_{III}) for cases 0 and 1–4; crack inclination $\phi = 30°$. [$a = 0.254$ m (1 in.), $\sigma = 6895$ Pa (1 psi)].

where K_p is taken to represent the stress intensity at which the crack propagates and is considered to be a material-dependent function of the orientation of the crack tip consistent with the regime of crack growth. Kfouri (1996) proposed the elliptical form shown below:

$$\frac{1}{K_p(\theta)^2} = \frac{\cos^2\theta}{K_p(0^\circ)^2} + \frac{\sin^2\theta}{K_p(90^\circ)^2} \tag{15}$$

Either case produces a nearly identical oblong shape in polar coordinates for fairly small orthotropy ratios, as illustrated in Fig. 15 (Pettit, 2000).

Extension of 2D fracture orthotropy relations to 3D is not straightforward, nor is there an established or accepted method to do so. Pettit (2000) accounts for three-dimensional orthotropy by defining a function that interpolates the fracture resistance for arbitrary orientations in terms of six principal fracture toughness values, and we have adapted his approach to the foam material. In a three-dimensional body a crack may be non-planar, and oriented arbitrarily. At any point along the crack front in an orthotropic material, however, we can characterize the local orientation in terms of the tangent plane and the crack front normal vector within that plane, defined relative to the principal axes of the material. For an orthotropic material there are three orthogonal planes of symmetry. Within each of these planes there are thus two orthogonal axes of symmetry. This results in six principal fracture toughness values. The material is assumed to be homogeneous, thus the toughness for a given orientation relative to these principal planes is invariant with regard to translation. Following the convention established for metals (Goode, 1972), the principle values of fracture toughness are written in a two-letter code (i–j) where the first letter refers to the principle axis normal to the crack plane, and the second subscript identifies the principle axis corresponding to the direction of propagation. The six principal toughness values are defined in Fig. 16, for a crack rotated arbitrarily relative to the material orientation. The crack (or a point on an arbitrary crack front) may propagate in an arbitrary direction defined by unit vector $\mathbf{a} = a_1\mathbf{i} + a_2\,\mathbf{j} + a_3\mathbf{k}$, where $\mathbf{i}$, $\mathbf{j}$, and $\mathbf{k}$ are unit vectors corresponding to the principal material axes. Vector $\mathbf{a}$ lies within a plane tangent to the developing crack surface at the crack front, which plane is uniquely described by its unit normal vector $\mathbf{n} = n_1\mathbf{i} + n_2\,\mathbf{j} + n_3\mathbf{k}$. The crack orientation is uniquely defined by the direction cosines a_i and n_i. Following the work of Buczek and Herakovich (1985), the interpolation function must, (i) be independent of a_i and n_i for an isotropic material, and (ii) return the principal fracture resistances for cracks in the corresponding principal orientations. Seeking the lowest order function that can achieve this that also reverts to the two-dimensional form of Eq. (14), Pettit (2000) derives the fracture resistance components of $\mathbf{a}$ in the principal planes as

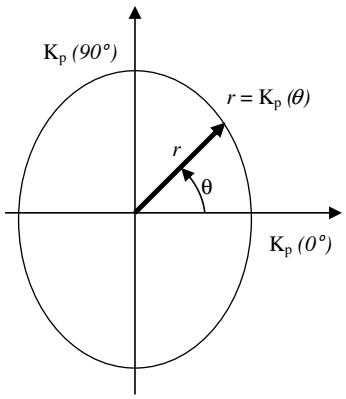

Fig. 15. Assumed elliptical function describing two-dimensional crack growth resistance as a function of orientation for materials with fracture orthotropy.

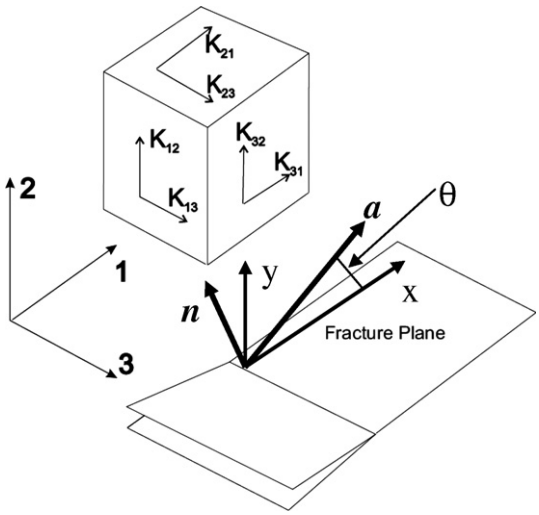

Fig. 16. Anisotropic toughness [Pettit, 2000].

$$
\begin{aligned}
K_1(\mathbf{a}) &= \frac{1}{1-a_1^2}\left(K_{12}a_2^2 + K_{13}a_3^2\right)\\
K_2(\mathbf{a}) &= \frac{1}{1-a_2^2}\left(K_{23}a_3^2 + K_{21}a_1^2\right)\\
K_3(\mathbf{a}) &= \frac{1}{1-a_3^2}\left(K_{31}a_1^2 + K_{32}a_2^2\right)
\end{aligned}
\tag{16}
$$

These components are summed in some weighted combination based on crack-plane normal **n** to obtain the effective fracture resistance, $K_p(\mathbf{a}, \mathbf{n})$ or $K_{eff}(\mathbf{a}, \mathbf{n})$. Since the weight factors must sum to unity to satisfy the isotropic case, Pettit (2000) expresses the effective fracture resistance as

$$
\begin{aligned}
K_p(\mathbf{a},\mathbf{n}) &= K_{eff}(\mathbf{a},\mathbf{n}) = K_1 n_1^2 + K_2 n_2^2 + K_3 n_3^2\\
&= \frac{n_1^2}{1-a_1^2}\left(K_{12}a_2^2 + K_{13}a_3^2\right) + \frac{n_2^2}{1-a_2^2}\left(K_{23}a_3^2 + K_{21}a_1^2\right) + \frac{n_3^2}{1-a_3^2}\left(K_{31}a_1^2 + K_{32}a_2^2\right)
\end{aligned}
\tag{17}
$$

Using the mode I toughness values measured in the three principal directions [$K_{12} = 23\ \text{psi}\sqrt{\text{in.}}(25,057\ \text{Pa}\sqrt{\text{m}})$, $K_{13} = 17.4\ \text{psi}\sqrt{\text{in.}}(19,122\ \text{Pa}\sqrt{\text{m}}), K_{21} = 19.5\ \text{psi}\sqrt{\text{in.}}(21,430\ \text{Pa}\sqrt{\text{m}})$], we use Eq. (17) to estimate toughness in an arbitrary direction. For the transversely isotropic material we have three unique toughness values and are taking $K_{23} = K_{13}$, $K_{31} = K_{21}$, and $K_{12} = K_{32}$. We note that we are only making use of the mode I toughness values measured in the three principal 11, 22 and 33 directions. We have omitted the use of K_{II} and K_{III} since there is no accepted three-dimensional fracture criterion for anisotropic material under mixed-mode loading conditions. For arbitrary crack angles and material orientations, K_{II} and K_{III}

are expected to play a role in determining both K_{eff} and crack turning angle. The fracture criterion based on Eq. (17) is a first attempt at evaluating fracture properties of anisotropic foam, a material of engineering importance. Efforts should be made in the future to include mode mixity effects for formulating fracture criterion for anisotropic materials.

7. Crack turning angle

Predicting crack turning angle under mixed-mode loading for anisotropic materials is a complex endeavor involving the calculation of the stress and displacement fields near the crack tip and accounting for the direction dependence of both the elastic and fracture properties. The three theories prevalent in the literature to predict incipient crack turning angles for isotropic materials are the maximum hoop stress [Erdogan and Sih, 1963], maximum energy release rate (Hussain et al., 1974), and minimum strain energy density [Sih, 1974].

Buczek and Herakovich (1985) were among the first to predict the crack extension angle for orthotropic composite materials. Nobile and Carloni (2005) and Carloni et al. (2003) consider incipient crack turning for an orthotropic plate under biaxial loading. Mixed-mode crack propagation in anisotropic materials is investigated by Saouma et al. (1987) based on Sih et al. (1965), under conditions of z-symmetry. Chen (1999) analyzed crack propagation in aluminum based on a ratio of the hoop stress to anisotropic fracture toughness, K_c. A similar analysis was conducted by Pettit (2000) for rolled aluminum, which has isotropic stiffness properties but anisotropic fracture characteristics defined by Eq. (17). Pettit (2000) predicted the anisotropic crack turning angle based on finding the maximum value of the function $\sigma_{\theta\theta}/K_{\text{eff}}(\boldsymbol{a},\boldsymbol{n})$ in the neighborhood of the crack tip, illustrated in Fig. 17.

The hoop stress $\sigma_{\theta\theta}$ in the neighborhood of the crack tip is calculated based on the general expressions for anisotropic materials shown below (Hoenig, 1982), and use of appropriate coordinate transformations:

$$\begin{Bmatrix} \sigma_{xx} \\ \sigma_{yy} \\ \sigma_{yz} \\ \sigma_{zx} \\ \sigma_{xy} \end{Bmatrix} = \frac{1}{\sqrt{2\pi r}} \begin{Bmatrix} \mathrm{Re}\left(\sum_{i=1}^{3} \frac{\mu_i^2 N_{ij}^{-1} K_j}{(\cos\theta+\mu_i \sin\theta)}\right) \\ \mathrm{Re}\left(\sum_{i=1}^{3} \frac{N_{ij}^{-1} K_j}{(\cos\theta+\mu_i \sin\theta)}\right) \\ -\mathrm{Re}\left(\sum_{i=1}^{3} \frac{\mu_i N_{ij}^{-1} K_j}{(\cos\theta+\mu_i \sin\theta)}\right) \\ \mathrm{Re}\left(\sum_{i=1}^{3} \frac{\mu_i \lambda_i N_{ij}^{-1} K_j}{(\cos\theta+\mu_i \sin\theta)}\right) \\ -\mathrm{Re}\left(\sum_{i=1}^{3} \frac{\lambda_i N_{ij}^{-1} K_j}{(\cos\theta+\mu_i \sin\theta)}\right) \end{Bmatrix} \tag{18}$$

$$\sigma_{zz} = -(S_{31}\sigma_{xx} + S_{32}\sigma_{yy} + S_{34}\sigma_{yz} + S_{35}\sigma_{zx} + S_{36}\sigma_{xy})/S_{33}$$

Fig. 18 shows a fractured M(T) test specimen. The wavy knit lines are marked by dots. The waviness results from difficulty in spraying in a straight line and also the rise heights differ along the spray line. An average knit line angle nearest to the crack was used to determine the orientation of the material coordinate axes (x', y', z'), shown in Fig. 19. Test results from

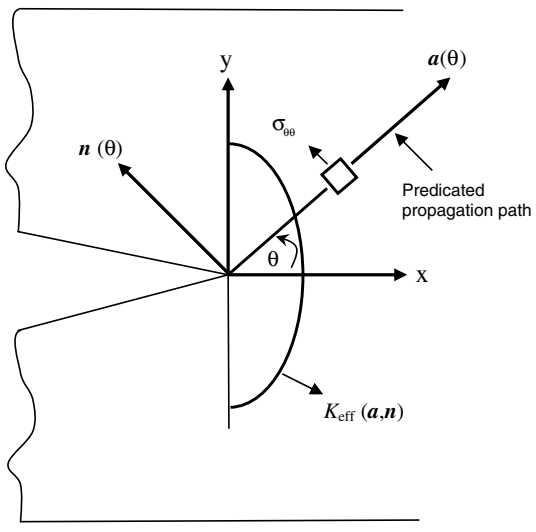

Fig. 17. Criteria for predicting anisotropic crack turning angle (Pettit, 2000).

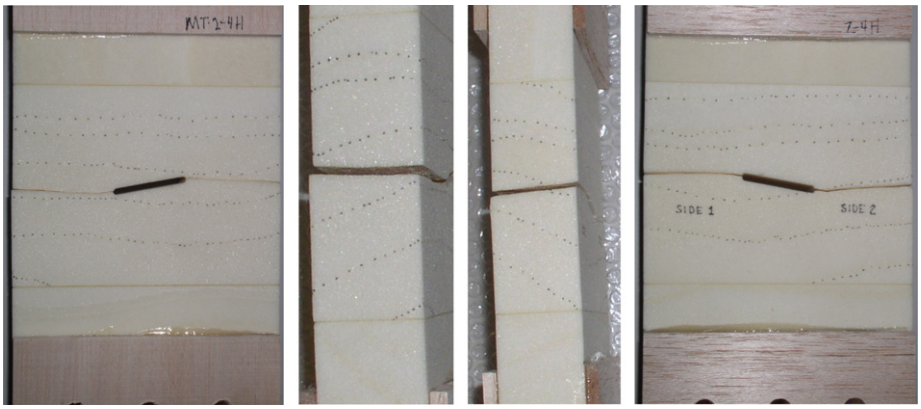

Fig. 18. From left to right: front, left, right, and rear sides of the fractured M(T) specimen.

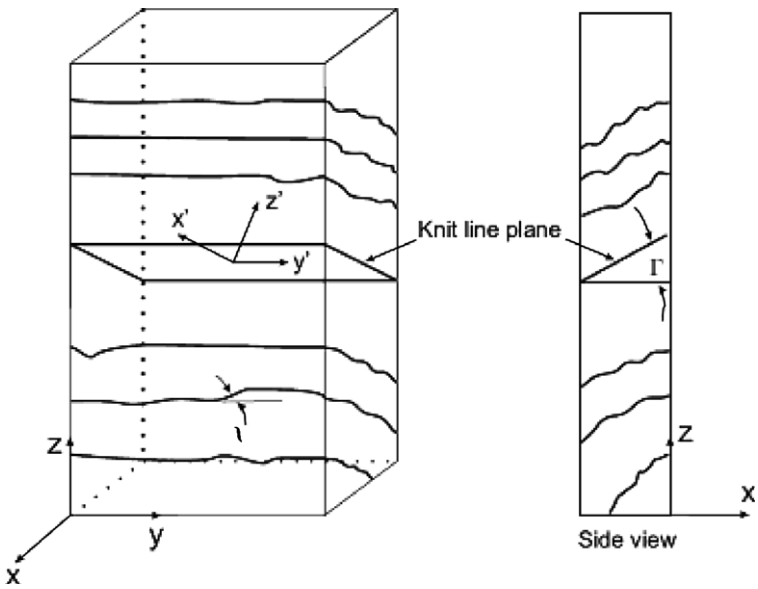

Fig. 19. Definition of the knit line plane and orientation of material coordinate axes (x', y', z') The procedure for predicting anisotropic crack turning angle is summarized below (Knudsen, 2006).

three M(T) specimens, labeled A–C, are used to predict crack turning angles. Fabrication of the M(T) specimens involves spraying the foam on a metal plate, slowing it to rise and form a rind or knit line. When the foam has settled, the next layer is applied until the desired thickness is achieved. From here, the foam is cut from this parent block so the knit lines are running in the desired directions.

The direction cosines for the material coordinate systems of specimens A–C are shown in Table 3. Note that because of the wavy nature of the knit lines, determination of the direction cosines for the material axes is approximate. The angles ψ and Γ

Table 3
Direction cosines for the material coordinate axes for specimens A–C

	Specimen A			Specimen B			Specimen C		
	x	y	z	x	y	z	x	y	z
x′	0.94	0	−0.342	−0.94	0	−0.342	0.77	0	0.64
y′	0	1	0	0	0.984	0.174	0.09	0.99	−0.1
z′	0.342	0	0.94	0.337	0.163	−0.925	−0.632	0.133	0.76

Table 4
Measured and predicted crack turning angles

	Crack inclination, ϕ	θ_c (measured)	θ_c (predicted)	θ_c (isotropic)
Specimen A	10°	27	32	43
Specimen B	10	9.7	21	27
Specimen C	30	12	19	27

define the knit line plane, as shown in Fig. 19, and ϕ defines the crack inclination angle. The crack inclinations for specimens A–C are 10°, 10° and 30°. The direction cosines between the (x, y, z) and (x', y', z') coordinates are obtained by successive rotations about the unprimed and primed axes, to arrive at the final (x', y', z') configuration.

The procedure for predicting anisotropic crack turning angle is summarized below (Knudsen, 2006):

- Run the ANSYS FE model with the appropriate material orientation and compute the SIFs (K_I, K_{II}, K_{III}) using FRANC3D.
- Rotate material properties into a local crack front coordinate system
- Compute near-tip stresses using Eq. (11) (Hoenig, 1982).
- Compute $\sigma_{\theta\theta}$ using near-tip stresses and appropriate coordinate transformations.
- Determine the angle θ at which the function $\sigma_{\theta\theta}/K_{\text{eff}}(\boldsymbol{a}, \boldsymbol{n})$ reaches a maximum value, to predict the crack turning angle, θ_c.

Table 4 presents measured and predicted crack turning angles for specimens A–C. Turning angles based on isotropic assumptions are also presented. The SIFs can vary along the crack front and since the free surface can influence the numerical K-solution, the measured and predicted angles are shown for the specimen mid-plane. The turning angle was measured using a Brown and Sharpe coordinate measuring machine. Specimen A has the best agreement between measured and predicted results. Errors can result from the measurement of the material coordinate axes. When defining the knit line plane, the knit line closest to the crack was used to define the orientation, even though the material orientation can vary over the specimen. For the three specimens tested, the crack tends to turn in the mode I direction, perpendicular to the max principal stress direction. More testing is required to generalize results.

The K_{eff} expression used (Eq. (17)) does not include the effects of mode mixity arising from K_{II} and K_{III}. Inclusion of effects of mixed-mode loading may result in better agreement between experimental and calculated results for the crack propagation angle.

8. Conclusions

Comprehensive results for anisotropic mixed-mode SIFs (K_I, K_{II}, K_{III}) for BX-265 foam material, used for insulating the shuttle cryogenic external tank, are presented. Based on experimental test data, this foam material is modeled as transversely isotropic linear elastic solid. We present a general procedure for computing mixed-mode SIFs for anisotropic materials. Middle-tension M(T) finite element models with 17 different material orientations were analyzed and the mixed-mode SIFs (K_I, K_{II}, K_{III}) were computed using FRANC3D software developed by the Cornell University Fracture Group. The SIFs are presented as a function of specimen through thickness, and crack inclination, for 17 material orientations. We observe that even when the material primary axis was offset by 45°, K_I varied by only 14%, indicating that toughness is not a strong function of material orientation. We present fracture toughness values for the foam material in three primary directions and also a means for evaluating directional dependence of anisotropic toughness based on work by Pettit (2000). A detailed procedure for predicting anisotropic crack turning angles is presented and theoretical predictions are compared with measured values.

The results presented, based on comprehensive numerical and experimental investigations, represent a quantitative basis for evaluating the strength and fracture properties of BX-265 anisotropic foam material, used to insulate the space shuttle external tank. Inclusion of mixed-mode loading effects for determining K_{eff} for anisotropic materials is recommended for future work.

Acknowledgments

This work was supported by the NASA Marshall Space Flight Center, Huntsville, AL. Discussions on theoretical aspects and finite element modeling of cracks in anisotropic materials with Drs. B. Carter and P. Wawrzynek of the Cornell University Fracture Group, and Dr. R. Pettit at Pratt & Whitney, East Hartford, CT, has contributed greatly towards our understanding and completion of this work.

References

Aliabadi, Rooke, D.P., 1991. Numerical Fracture Mechanics. Computational Mechanics Publications, Boston. 45 pp.
ANSYS Elements Reference, 1999. ANSYS Release 5.6, ANSYS Inc.

Banks-Sills, L., Hershkovitz, I., Wawrzynek, P.A., Eliasl, R., Ingraffea, A.R., 2005. Methods for calculating stress intensity factors in anisotropic materials. Part *I–z* = 0 is a symmetry plane. Engineering Fracture Mechanics 72, 2328–2358.
Banks-Sills, L., Wawrzynek, P.A., Carter, B., Ingraffea, A.R., Hershkovitz, I., 2007. Methods for calculating stress intensity factors in anisotropic materials. Part II. Arbitrary geometry. Engineering Fracture Mechanics 74, 1293–1307.
Buczek, M.B., Herakovich, C.T., 1985. A normal stress criterion for crack extension direction in orthotropic composite materials. Journal of Composite Materials 19, 544–553.
Carloni, C., Piva, A., Viola, E., 2003. An alternative complex variable formulation for an inclined crack in an orthotropic medium. Journal of Engineering Fracture Mechanics 70, 2033–2058.
Chen, C.S., 1999. Crack growth simulation and residual strength prediction in thin shell structures. Ph.D. Dissertation, Cornell University.
Erdogan, F., Sih, G.C., 1963. On the extension of plates under plane loading and transverse shear. Journal of Basic Engineering 85, 519–527.
FRANC3D Concepts and Users Guide, 2003. Available from the Cornell Fracture Group website (http://www.cfg.cornell.edu), Ithaca.
Freed, Y., Banks-Sills, L., 2005. A through interface crack between a ±45° transversely isotropic pair of materials. International Journal of Fracture 133 (1), 1–44.
Goode, R.J., 1972. Identification of fracture plane orientation, materials research and standards (MIRSA). ASTM 12 (9).
Hoenig, A., 1982. Near-tip behavior of a crack in a plane anisotropic elastic body. Engineering Fracture Mechanics 16 (3), 393–403.
Hussain, M.A., Pu, S.L., Underwood, J.H., 1974. Strain energy release rate for a crack under combined mode I and mode II. Fracture Analysis ASTM STP 560, 2–28.
Ishikawa, H., 1980. A finite element analysis of stress intensity factors for combined tensile and shear loading by only a virtual crack extension. International Journal of Fracture 16, 243–246.
Kfouri, A.P., 1996. Crack extension under mixed-mode loading in an anisotropic mode-asymmetric material in respect of resistance to fracture. Fatigue & Fracture of Engineering Materials & Structures 19 (1), 27–38.
Knudsen, E.C., 2006. Anisotropic fracture analysis of BX-265 foam insulation material under mixed-mode loading. Ph.D. Dissertation, Mechanical & Aerospace Engineering Department, University of Florida, Gainesville, FL.
Knudsen, E.C., Arakere, N.K., 2006. Numerical evaluation of Mode I stress intensity factor for BX-265 foam insulation material. Presented at the 51st ASME/IGTI Turbo Expo International Conference, Barcelona, Spain, May 8–11, 2006.
Lemant, F., Pineau, A., 1981. Mixed mode fracture of a brittle orthotropic material – example of strongly textured zinc sheets. Engineering Fracture Mechanics 14, 91–105.
Li, F.Z., Shih, C.F., Needleman, A., 1985. A comparison of methods for calculating energy release rates. Engineering Fracture Mechanics 21, 405–421.
Nobile, L., Carloni, C., 2005. Fracture analysis for orthotropic cracked plates. Journal of Composite Structures 68, 285–293.
Parks, D.M., 1974. A stiffness derivative finite element technique for the determination of crack tip stress intensity factors. International Journal of Fracture 10 (4).
Pettit, R.G., 2000. Crack turning in integrally stiffened aircraft structures. Ph.D. Dissertation, Cornell University, Ithaca, NY.
Raju, I.S., 1987. Calculation of strain energy release rates with higher order and singular finite elements. Engineering Fracture Mechanics 28 (3), 251–274.
Ranjan, S., Arakere, N.K., 2008. A fracture mechanics based methodology for fatigue life prediction of single crystal nickel based superalloys. ASME Journal of Engineering for Gas Turbines and Power 130 (3), 032501, 1–11.
Rice, J.R., 1968. A path independent integral and the approximate analysis of strain concentration by notches and cracks. Journal of Applied Mechanics 35, 379–386.
Saouma, V.E., Ayari, M.L., Leavell, D.A., 1987. Mixed mode crack propagation in homogenous anisotropic solids. Journal of Engineering Fracture Mechanics 27, 171–184.
Shih, C.F., Moran, B., Nakamura, T., 1986. Energy release rate along a three-dimensional crack front in a thermally stressed body. International Journal of Fracture 30 (2), 79–102.
Sih, G.C., 1974. Strain energy density factor applied to mixed mode crack problems. International Journal of Fracture 10, 321–350.
Sih, G.C., Paris, P.C., Irwin, G.R., 1965. On cracks in rectilinearly anisotropic bodies. International Journal of Fracture Mechanics 1, 189–202.
Swenson, D., Ingraffea, A., 1987. A finite element model of dynamic crack propagation with an application to intersecting cracks. In: Proceedings of the Fourth International Conference on Numerical Methods in Fracture Mechanics. San Antonio, TX.
Swenson, D., Ingraffea, A., 1988a. Modeling mixed-mode dynamic crack propagation using finite elements: theory and applications. Computational Mechanics 3, 187–192.
Swenson, D., Ingraffea, A., 1988b. Using combined experiments and analysis to generate dynamic critical stress intensity data. In: Cruse, T. (Ed.), Fracture Mechanics: 19th Symposium, vol. 969. ASTM STP, Philadelphia, pp. 405–426.
Ting, T.C.T., 1996. Anisotropic Elasticity-Theory and Applications. Oxford University Press. pp. 34–37.
Yau, J.F., Wang, S.S., Corten, H.T., 1980. A mixed-mode crack analysis of isotropic solids using conservation laws of elasticity. ASME Journal of Applied Mechanics 47, 335–341.